Conformal Coating by High Pressure Chemical Deposition for Patterned Microwires of II–VI Semiconductors

*Justin R. Sparks, Rongrui He, Noel Healy, Subhasis Chaudhuri, Thomas C. Fitzgibbons, Anna C. Peacock, Pier J. A. Sazio, and John V. Badding**

Deposition techniques that can uniformly and conformally coat deep trenches and very high aspect ratio pores with uniform thickness films are valuable in the synthesis of complex three-dimensionally structured materials. Here it is shown that high pressure chemical vapor deposition can be used to deposit conformal films of II–VI semiconductors such as ZnSe, ZnS, and ZnO into high aspect ratio pores. Microstructured optical fibers serve as tailored templates for the patterning of II–VI semiconductor microwire arrays of these materials with precision and flexibility. In this way, centimeters-long microwires with exterior surfaces that conform well to the nearly atomically smooth silica templates can be fabricated by conformal coating. This process allows for II–VI semiconductors, which cannot be processed into optical fibers with conventional techniques, to be fabricated into step index and microstructured optical fibers.

1. Introduction

Conventional atmospheric to sub-atmospheric pressure chemical vapor deposition (CVD) techniques are well suited for the fabrication of planar thin films. However, they are limited in their ability to uniformly and conformally coat and/or fill extreme aspect ratio voids and trenches with well-developed, uniform thickness films. The ability to conformally coat these features is of particular value in the synthesis of geometrically complex, three-dimensional materials that are hierarchically organized across a range of length scales. Deposition of successive conformal, nanoscale thickness layers of unary semiconductors within selected micrometers diameter pores of optical fiber templates has been shown to allow for precise organization of materials in these pores, for example.[1] Additional examples where the coating of complex templates is valuable include pillar array photovoltaics,[2] intricate microfluidic channels and in-channel microfluidic devices,[3] nanoscale biological templates,[4] 3D optical metamaterials,[5] and 3D electronics.

Atomic layer deposition (ALD) has been the most viable technique for conformally coating high aspect ratio micro/nanostructures with semiconductors because the self-limiting nature of the deposited film allows for uniform film thickness despite variations in the precursor flux to the surface.[6,7] However, the requirement for self-limited chemical reaction and thermal stability at the desired growth temperature places limits on the range of precursor molecules that can be employed and thus also the accessible materials. Moreover, the layer-by-layer nature of the process greatly limits the overall rate of deposition.[8,9]

CVD allows for higher rates of deposition of semiconductor materials than ALD and does not require self-limited chemical reactions. The poor ability of conventional CVD to conformally coat deep nanoscale size voids or pores with semiconductors arises because the mean free path for molecules at the atmospheric or sub-atmospheric pressures typically employed is hundreds of nm or more, such that effusion of molecules into nanoscale openings is the primary transport mechanism. Thus the transport into these openings is relatively slow. However, at high pressures, on the order of tens of MPa, the molecular mean free path is on the order of a nanometer, allowing for pressure driven transport by hydrodynamic flow into micro/nanoscale voids. The rate of mass transport to micro/nanoscale voids and features then becomes nearly equal to the rate of transport to macroscale features. Thus high pressure CVD (HPCVD) can conformally coat surfaces with semiconductor films yet still allow for a higher rate of deposition than ALD and wide range of precursor chemistries possible with CVD.

II–VI structures in bulk, thin film, nanowire, and quantum dot geometries have been reported. We have previously reported the deposition of nearly void-free microwires of ZnSe in a single silica capillary via HPCVD for single core optical fiber applications.[10] Here we describe the conformal coating of the very high aspect ratio pores in silica microstructured optical fiber (MOF) templates with the II–VI materials ZnS and $ZnS_xSe_{(1-x)}$ via HPCVD. This coating proceeds such that precisely patterned, centimeters-long arrays of wires micrometers in diameter can be formed. These Zn chalcogenide

J. R. Sparks, Dr. R. He, S. Chaudhuri,
T. C. Fitzgibbons, Prof. J. V. Badding
Department of Chemistry and
Materials Research Institute
Pennsylvania State University
University Park, PA 16802, USA
E-mail: jbadding@chem.psu.edu
Dr. N. Healy, Dr. A. C. Peacock, Dr. P. J. A. Sazio
Optoelectronics Research Centre
University of Southampton
Highfield, Southampton SO17 1BJ, UK

DOI: 10.1002/adfm.201202224

semiconductors are useful for their wide range of transparency from visible to mid-infrared wavelengths, their refractory nature that makes them resistant to damage from high optical intensities,[11] their wide direct bandgaps that allow for UV light emission and detection, and their infrared fluorescence[12] and large Verdet constants[13] when appropriately doped. $ZnS_xSe_{(1-x)}$ is of particular interest because properties such as its refractive index can be continuously tuned with x over a wide range. Importantly, alloying opens up the possibility to fabricate optical fibers with small core-cladding index contrasts through the deposition of successive layers with varying x, or alternatively, to tune the index contrast in complex 2D photonic crystal structures to shift the positions of the bandgaps. Furthermore, the lattice constant in $ZnS_xSe_{(1-x)}$ alloys can also be controlled to allow for continuous tuning of their direct bandgap from 2.7 to 3.6 eV, allowing for emission of light from the visible to the near UV.[32] We also show that extreme aspect ratio structures composed of these materials can serve as templates that can be oxidized to another compound semiconductor that has found a wide range of applications, ZnO.[14]

The microwires fabricated via HPCVD adopt the near atomically smooth surface roughness of their silica capillary templates[15] and have very uniform cross-sectional diameters along their length. Such geometric perfection and low surface roughness is critical to transport of photons and electrons without detrimental losses due to processes such as scattering.[16] Patterning individual elements such as wires into arrays as demonstrated here allows for new functions to be incorporated into devices, including photonic bandgaps,[17] coherent beam combining,[18] high resolution infrared chemical imaging,[19] and unique light coupling schemes between silica and semiconductors.[1] As a specific example application, we demonstrate the first microstructured ZnSe optical fiber with robust dual mode guidance.

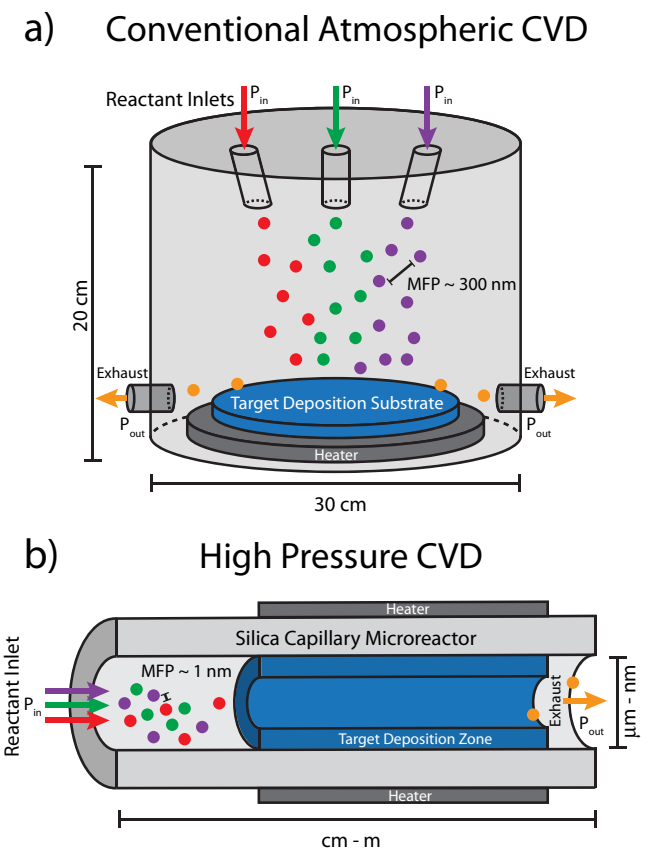

Figure 1. a) Schematic of atmospheric CVD process, where source molecules can be introduced to a heated substrate separately such that prereaction can, in general, be avoided. Flow towards the substrate is achieved via a small pressure difference with the exhaust ports. b) Schematic of HPCVD in a capillary microreactor, where a high pressure precursor mixture of source molecules is configured to flow into a capillary (left) with the opposite end open to atmosphere (right). In the unheated region of the capillary, precursor molecules are so intimately mixed that any tendency to prereact at low temperatures must be avoided. When the capillary is heated, well-developed annular films are deposited, while unreacted precursors, carrier gas, and reaction byproducts are exhausted downstream.

2. Results and Discussion

2.1. A General High Pressure CVD Approach for Coating Very High Aspect Ratio Templates

Nearly every aspect of the overall pathway from molecular precursor to a desired material film in HPCVD is different from conventional CVD in view of the high pressures employed. Chemical thermodynamics is altered by volume-pressure term ($V\Delta P$) in the expression for the Gibbs free energy[20] while kinetics are altered by the vastly increased molecular collision rates associated with nanoscale mean free paths.[21] Large pressure differences and confined geometries alter reactant diffusion as well as the flow,[22] especially in the all-important boundary layer in the immediate vicinity of the surface chemical reaction.[23] All of these factors must be considered when choosing a chemical reactor geometry and precursor chemistry for HPCVD of well-developed, conformal films.

An important practical difference in HPCVD is that reaction precursors must often be transported together for delivery into a heated reaction zone whereas conventional CVD reactors typically allow for the introduction of precursors separately to avoid prereaction before they reach a planar deposition target (**Figure 1**a).[24] Thus the precursors selected for HPCVD must be chosen so that they do not prereact as they are transported to a desired deposition location at low temperature, yet do react once they reach it and are heated. Another challenge is that the deposition characteristics can change as a void is filled with semiconductor because the precursor flow rate is altered as a result of the changes in geometry due to pore closure. Polycrystalline grain growth, in particular, is affected by the mass transport rate to the surface.[25]

We find that the organometallic molecules R_2Zn, R_2S, and R_2Se, where R = alkyl, are particularly suitable for HPCVD of II–VI semiconductors. These liquid precursors have appreciable vapor pressures, making them viable for vapor deposition reactions,[26,27] but they do not introduce as many impurities as solid, single source precursors with complex aryl-carbon ligands.[28] Furthermore, the precursor reactivity can be controlled

by tuning of the metal-carbon bond strengths with different R groups. For example, branched t-butyl groups allow for lower reaction temperatures.[29] These alkyl precursors also do not suffer from room temperature prereactions in contrast to the $R_2Zn/H_2S/H_2Se$ precursors commonly employed for zinc chalcogenide CVD.[24] R_2S and R_2Se are weaker Lewis bases that do not react as readily with the Lewis acid alkyl zinc. Instead, the reactive, intermediate chalcogenide hydrides are formed in situ at the desired deposition location by reaction between alkylchalcogenides and H_2 (Reaction 2). We chose R = methyl precursors because they are volatile and readily available in pure form. The following reaction steps are thought to occur at the targeted deposition site:[30]

$$(CH_3)_2Zn + H_2 \rightarrow Zn + 2CH_4 \quad (1)$$

$$(CH_3)_2S/(CH_3)_2Se + 2H_2 \rightarrow H_2S/H_2Se + 2CH_4 \quad (2)$$

$$Zn + H_2S/H_2Se \rightarrow ZnS/ZnSe + H_2 \quad (3)$$

Thus the organometallic precursors "encapsulate" the more reactive Zn and H_2S/H_2Se species until the reaction temperature is high enough to induce Reactions 1 and 2, followed by 3.

In a typical deposition, the volatile organometallic precursor mixture is pressurized with hydrogen, which functions as a reactant and carrier, to a total pressure of 35–70 MPa and configured to flow through a heated (400–500 °C) capillary (Figure 1b) with the opposite end open to atmospheric pressure. The pressure differential between the ends allows for the transport of the precursor molecules into the high aspect ratio pores. When the MOF is heated, a heterogeneous reaction occurs on the surface of the silica capillaries with a typical precursor conversion efficiency of ≈15%[10] while the reaction byproducts, such as methane, unreacted precursors, and carrier gas are exhausted downstream. The conformal nature of the early stages of deposition is highlighted in **Figure 2**a. The film continues to become thicker and the interior pore decreases in diameter as the reaction proceeds.

ZnS layers form by the reaction of $(CH_3)_2S$ and $(CH_3)_2Zn$ and the ZnSe layers form by the reaction of $(CH_3)_2S$ and $(CH_3)_2Zn$ in 15 µm capillaries (Figure 2b). The layers are transparent and conformally coat the capillaries so well that at the end of the deposition the remaining central void is about 500 nm in diameter (Figure 2c). In this way structures that are nearly void-free microwires are formed by conformal coating; we consider them to be nearly void-free because the majority of the 15 µm diameter capillary is filled. The central void appears much larger than it actually is in the optical microscopy images because it is magnified by cylindrical lensing. This interior pore is irregular in shape (Figure 2c), due to the polycrystalline grain growth, and ranges from 400 nm to 500 nm across.

The methane byproduct in the II–VI deposition reaction builds up in the pore once it clogs; with no way of exhausting it, the forward reaction becomes inhibited. The microwires can be several centimeters long (Figure 2d), much longer than it is typically possible to make ZnSe and ZnS micro/nanowires. Thus the aspect ratio of the central ≈500 nm nanopore is ≈10^5

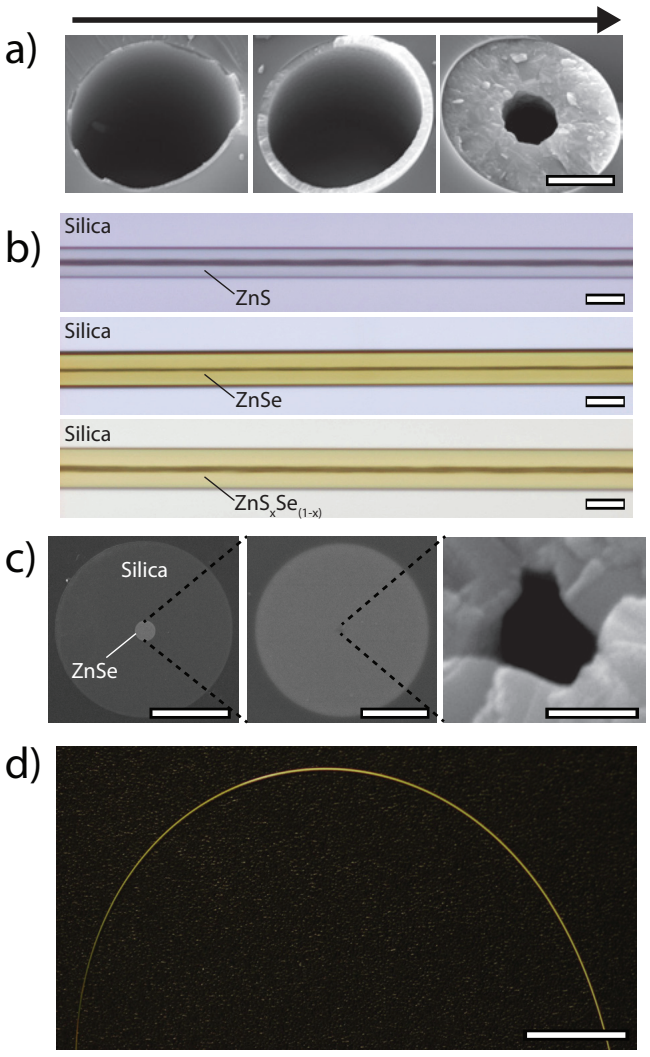

Figure 2. a) SEM images of the HPCVD process as it progresses and conformally coats the inner surface of a silica capillary. b) Diascopically illuminated optical microscopy images from the side showing transparent, uniform ZnS, ZnSe, and $ZnS_xSe_{(1-x)}$ deposited in silica micro-capillaries. c) Overview (left) and higher magnification (right) cross-sectional SEM images of a ZnSe infiltrated capillary showing the <500 nm remaining interior pore. d) Photograph of ZnSe microwires being bent while embedded in the silica MOF. Scale bars: a) 2 µm; b) 20 µm; c) left: 40 µm, middle: 4 µm, right: 500 nm; and d) 5 mm.

when deposition is halted by termination of flow, illustrating the ability of HPCVD to transport precursors into very deep voids. We note that as the aspect ratios of trenches in planar semiconductor structures are orders of magnitude less, HPCVD is also likely to be useful for coating these structures because the constraints for removal of reaction byproduct will be much less severe.

2.2. Materials Characterization

The deposited materials were determined to be polycrystalline and single phase via both powder X-ray diffraction (**Figure 3**)

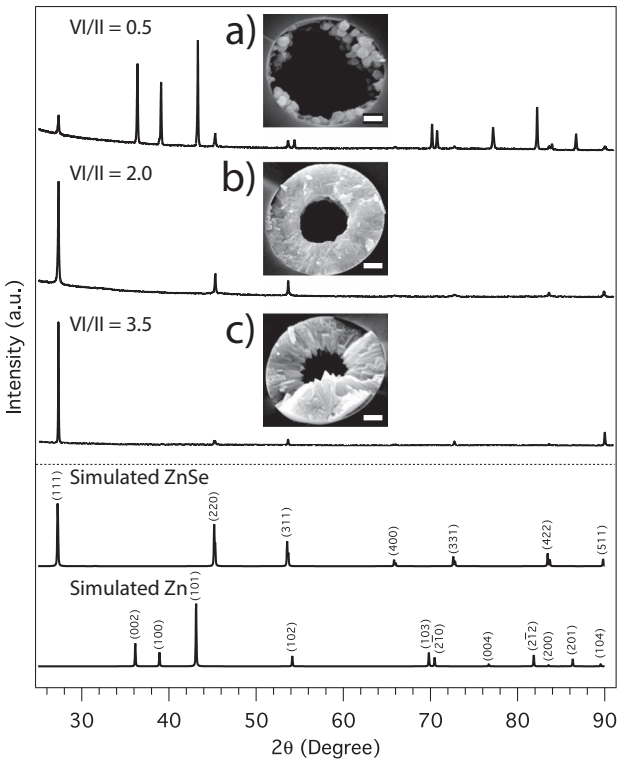

Figure 3. X-ray diffraction (Cu Kα) reveals the composition/morphology dependence on precursor ratio for ZnSe deposition. When the VI/II precursor ratio is too low (<1), a ZnSe film is deposited along with metallic Zn islands (a). Complete conversion of Zn to ZnSe with minimal texturing occurs when the ratio is >1 (b), while a high ratio (>2.5) results in columnar growth in the (111) direction (c). Inset SEM image scale bars: 1 μm.

and Raman spectroscopy (**Figure 4**). ZnS and ZnSe are both in the cubic zinc blende phase (Figure 3). The morphology, composition, and crystallinity of the deposited ZnSe material are very sensitive to the stoichiometric ratio of the precursors in the reactant flow (Figure 3). Only a very narrow range of stoichiometry gave rise to well developed conformal films. Similar trends were also observed for ZnS and $ZnS_xSe_{(1-x)}$.

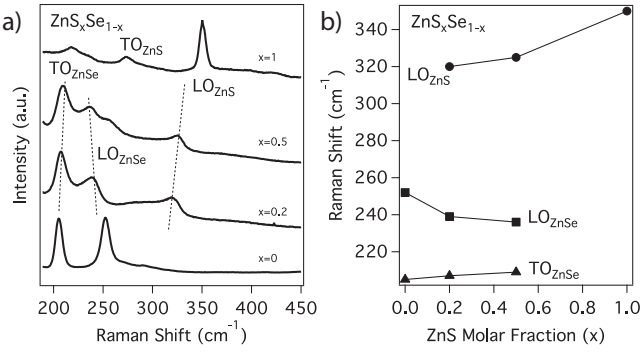

Figure 4. a) Raman spectroscopy of $ZnS_xSe_{(1-x)}$ alloys with 488 nm excitation. b) The shifts of the TO_{ZnSe}, LO_{ZnSe}, and TO_{ZnS} phonon modes are characteristic of alloy formation.

This sensitivity to precursor stoichiometry arises from the different kinetic rate constants for Reactions 1 and 2. When the VI/II precursor ratio is low (<1), a ZnSe film is deposited along with metallic Zn islands (Figure 3a). Complete conversion of Zn to ZnSe is achieved when the ratio is >1, with 2 being the best ratio with respect to morphology, texture, and stoichiometry (Figure 3b). A further increase of the ratio (>2.5) leads to columnar growth in the (111) direction, with a greater relative intensity of the (111) diffraction peak (Figure 3c). Elemental Se formation at even higher ratios (>5) is not observed, due to the high temperature needed for decomposition of H_2Se in H_2.[31] For ZnS deposition, the more stable sulfur-carbon bonds of the $(CH_3)_2S$ molecule result in a smaller Reaction 2 rate constant, requiring a higher VI/II ratio (≈10).

2.3. $ZnS_xSe_{(1-x)}$ Alloying

By introduction of both $(CH_3)_2Se$ and $(CH_3)_2S$ into the reactant flow, solid solutions of ZnSe and ZnS can be deposited in well-developed layers (Figure 2b). The kinetic rate constants for decomposition of these two molecules differ, allowing the challenge of controlling the S to Se ratio of the $ZnS_xSe_{(1-x)}$ solid solution to be met by varying the temperature and precursor ratio. Although these materials can crystallize in either the hexagonal wurtzite structure or the cubic zinc blende structure as the composition is varied,[32] powder X-ray diffraction showed that only the cubic structure was formed in HPCVD when stoichiometries were varied over the entire range from $x = 0$ to $x = 1$. The S to Se ratio ($x/1–x$) determined by energy dispersive spectroscopy for materials deposited at different temperatures agreed well with that determined from the measured lattice parameters via Vegard's law. The Raman spectra of the deposited materials are characteristic of $ZnS_xSe_{(1-x)}$, exhibiting TO_{ZnSe}, LO_{ZnSe}, and LO_{ZnS} phonon modes that shift continuously with x (Figure 4a).[33,34] Although the TO_{ZnS} phonon is present in pure ZnS ($x = 1$) deposited by HPCVD, it is very weak in the $ZnS_xSe_{(1-x)}$ spectra, consistent with previous reports.[34] As the ZnS mole fraction is increased, the TO_{ZnSe} and LO_{ZnSe} modes shift towards each other, with the TO_{ZnSe} shifting up in frequency and the LO_{ZnSe} shifting down (Figure 4b). The LO_{ZnS} mode shifts to lower frequency as the Se concentration increases. The asymmetric broadening observed for it with increasing Se concentration has been attributed to a disordering effect.[35]

2.4. Hierarchically Ordered Arrays of II–VI Semiconductors

Patterning of individual nano/microscale semiconductor building blocks into more complex structures is a challenge that has attracted tremendous attention over the past two decades.[36] Although the structures presented in this work are on the order of micrometers diameters, HPCVD of II–VI semiconductors should be applicable to nanometer dimensions with further optimization, as we have already shown with unary semiconductors.[22] MOF templates with hundreds to tens of thousands of pores can be filled with II–VI semiconductors with HPCVD (**Figure 5**). In this way, arrays of large numbers

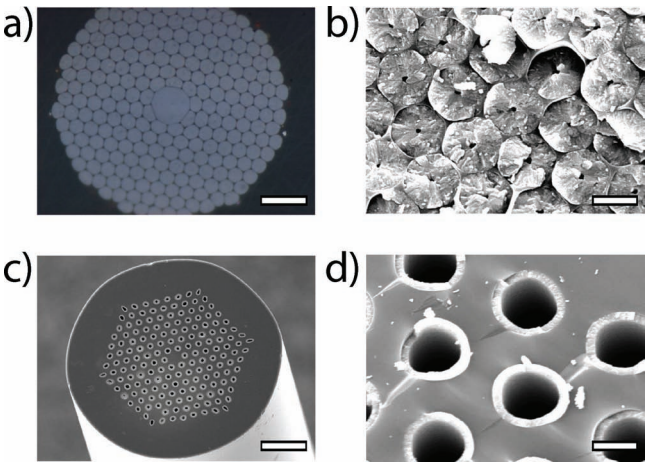

Figure 5. HPCVD in microstructured templates allows for precise positioning of hundreds of II–VI semiconductor microwires organized into complex arrays. a) Cross-sectional optical microscopy image of the polished facet of a ZnSe filled photonic bandgap optical fiber with a high packing density cladding shown in the SEM image (b). c) Cross-sectional SEM image of a lower packing density array filled with ZnSe tubes, as shown in higher magnification (d). Scale bars: a) 10 µm, b) 2.5 µm, c) 50 µm, and d) 5 µm.

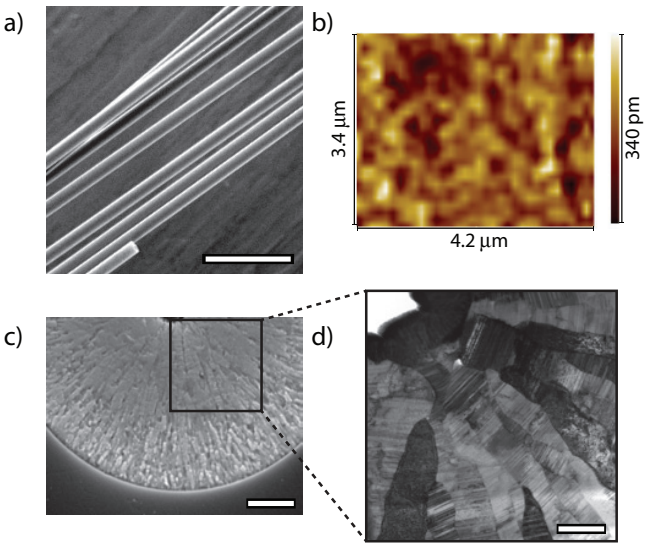

Figure 6. Surface roughness of ZnSe microwires. a) SEM image showing that II–VI microwires can be released from the template by HF etching to result in freestanding microwires. b) Optical interference profiling of a microwire that was removed from the template showing the near atomically smooth outer surface (0.1 nm RMS surface roughness). c) SEM image of NaOH grain boundary etching to reveal polycrystalline grain structure and size across the cross-section of a microwire, which determines the inner surface roughness of the interior pore. d) TEM image showing large grain structure near the central hole. Scale bars: a) 50 µm, c) 2 µm, and d) 500 nm.

of wires arranged in a wide range of very precise geometric patterns can be realized. The positions of the pores in the MOF templates can be controlled with nanometer level precision; furthermore these templates can be selectively filled,[37] allowing for much more accurate patterning of aligned ZnSe wires than has been possible with previously reported techniques.[38,39] ZnSe and ZnS nanowires made by CVD techniques tend to exhibit random "weed" growth because they typically involve non-templated/seeded growth that can result in wires and ribbons that are not straight.[40] Patterning techniques have been reported that allow for control over nanowire position,[41] but the geometric precision of the patterning and the geometric perfection of the wires themselves is much less than can be realized with MOF templates. The "outside-in" nature of the film growth to form wires via HPCVD allows the patterning to be defined by the MOF template. The wires formed are thus naturally straight and patterned with the high precision of the drawn template. As an example application of the patterning capability that thus arises, we filled the MOF template shown in Figure 5a with ZnSe, which has desirable optical properties discussed further in Section 2.6.

2.5. Structural Characterization of II–VI Microwires

The near atomically smooth (0.1 nm RMS roughness[15]) silica pore surfaces are coated with well-developed films from the "outside in". Thus it is important to first assess whether the microwires and tubes formed in these pores have comparable outer surface roughness.[42] We removed an array of 168 ZnSe wires 8 µm in diameter deposited in a silica template by etching with HF (**Figure 6**a). The surface roughness was characterized by means of optical interference profilometry, which uses interference between two split beams in a microscope to allow the RMS roughness to be determined over areal dimensions of hundreds of square micrometers with sub-Ångstrom sensitivity. We found that ZnSe microwires etched out of their template have a RMS surface roughness of 0.1 nm (Figure 6b), comparable to the surface roughness of the template walls. The capillary templates have extraordinary diameter uniformity along their length as well, such that variations of only tens of nanometers in diameter over lengths of centimeters are possible.[43] Since the ZnSe and ZnS microwires conform to the silica template walls, similar uniformity in diameter along their length can be expected.

Since the deposition results in a wire, or more specifically a tube with a very small central void, it is then important to assess this inner surface roughness. In contrast to hydride decomposition in silica capillaries,[22] the reaction chemistry of the II–VI semiconductor deposition does not yet allow for complete filling due to byproduct buildup, leaving behind a <500 nm diameter inner hole in the microwire. As the deposition progresses, the flow rate of reactants through the capillary decreases due to the growth of the polycrystalline film in the channel, resulting in a higher residence time of the precursors and the growth of larger grains which eventually forms a blockage and arrests deposition. The roughness of this inner surface will thus be determined by the grain size and shape at this interface. The cross sectional grain structure of the microwire is revealed by both grain boundary etching with NaOH (Figure 6c) and a TEM image (Figure 6d). We have found that changing the flow rate

via the pressure can provide control of this inner surface grain size and thus the remaining pore size. Further optimization of the reaction chemistry should result in a smoother, smaller inner pore, or even elimination of this central void.

No other technique has been reported that can make micro-scale diameter semiconductor wires of crystalline compound semiconductors such as ZnSe and ZnS with outer surfaces that are this smooth and uniform in diameter over lengths of centimeters with a circular cross section. Top-down lithographic methods, for example, typically result in semiconductor structures with varying diameters and several nanometers of surface roughness so that achieving 0.1 nm roughness is exceedingly difficult.[44,45] Just 1 to 2 nm of exterior surface roughness on a sub-micrometer-sized waveguide can significantly increase the scattering of visible and near infrared light transported within it.[46] Importantly, these ZnSe and ZnS microwires are likely to be useful as very high power laser cavities when suitably doped,[12] thus reducing the losses associated with surface scattering will be critical to achieving high net gains.

2.6. II–VI Semiconductor Step Index and Microstructured Optical Fibers

The Zn chalcogenide microwires function as relatively low optical loss crystalline semiconductor core optical fibers.[10,47,48] A summary of optical losses in semiconductor optical fibers at different wavelengths is given in reference 48. We have already reported losses of <1 dB/cm for 15 µm diameter core ZnSe optical fibers for wavelengths greater than 1000 nm.[10] For reference, semiconductor waveguides used for device demonstration typically have optical losses of <3 dB/cm. In contrast, ZnS microwires have a higher loss of 16 dB/cm, while the $ZnS_{0.2}Se_{0.8}$ microwires have a loss of 7 dB/cm. As the ZnS and $ZnS_xSe_{(1-x)}$ materials have comparable surface quality and crystallinity to ZnSe, it is likely that the larger losses measured in these materials can be attributed to impurity related absorption due to use of lower purity $(CH_3)_2S$; the $(CH_3)_2S$ was 99% pure versus electronic grade for $(CH_3)_2Se$ and $(CH_3)_2Zn$. When light is waveguided in microwires over centimeter distances, the presence of even small quantities of impurities can have an adverse effect on optical loss. With further development of precursor chemistry to reduce impurity levels, the optical losses in the sulfur-based materials should approach the loss values that have already been shown for ZnSe microwires.

In general, high refractive index semiconductor (n = 2.45 for ZnSe at 1550 nm) waveguides with either silica (n = 1.44) or air (n = 1) cladding have a large index contrast and thus are highly multimode. Realizing micrometer-sized semiconductor waveguides with more desirable low order mode or single mode behavior is still an ongoing challenge in photonics that requires proper refractive index grading. As previously mentioned, a key advantage of HPCVD in MOFs is the ability to deposit materials in complex 2D geometries to modify the guiding properties of light in the semiconductor wires. In particular, the structure shown in Figure 5a is the first demonstration of a ZnSe MOF, similar to the silicon MOF that was characterized,[49] which was shown to have a number of analogous properties to more standard air-silica MOFs. The fiber was fabricated by filling the air holes of a hollow core silica photonic bandgap fiber with ZnSe via HPCVD. The resulting structure has a 9 µm ZnSe core with a cladding of 3 µm ZnSe wires with ≈150 nm silica struts separating each wire. Compared to the step index fibers above, the ZnSe MOF has a cladding with a higher effective index than pure silica so that a reduced number of core modes can be selectively coupled. This ZnSe fiber is effectively dual mode over a wide wavelength range (**Figure 7**), though with further optimization of the MOF template and deposited material it should be possible to design a ZnSe MOF for effective single mode operation.[50] Transmission measurements in this microstructured ZnSe fiber at 1550 nm show it has a loss of 1.9 dB/cm. This slightly higher loss value than in a step index ZnSe optical fiber is likely to be due to the enhanced interaction of the core guided light with the high index microstructured cladding.

Likely sources of loss in the II–VI semiconductor optical fibers are geometric imperfections associated with the central void and material imperfections such as chemical impurities, grain boundaries and defects within grains. The presence of the central hole is certainly not desirable for optics applications as it can effect the mode structure of the waveguide and cause scattering.[10] The surface roughness of this interior pore is determined by the texture of the deposited film, which can be controlled and optimized via the reactant ratio (Figure 3). Higher pressure deposition at higher precursor concentrations and/or cycling the precursor pressure should allow for smaller pore diameters via smaller grain growth. Another approach to reducing the scattering of light associated with this central imperfection would be to increase the waveguide diameter to reduce the impact of the central pore on loss, which would require a cladding layer such as $ZnS_xSe_{(1-x)}$ (for a ZnSe core fiber) to be deposited first to reduce the index contrast (compared to silica cladding) and avoid the highly multimode nature of larger cores. Also, as can be seen in Figure 6d, there are many stacking faults and twinning defects in the material, which can cause scattering of light as it propagates through the structure. Thermal and laser annealing could reduce these

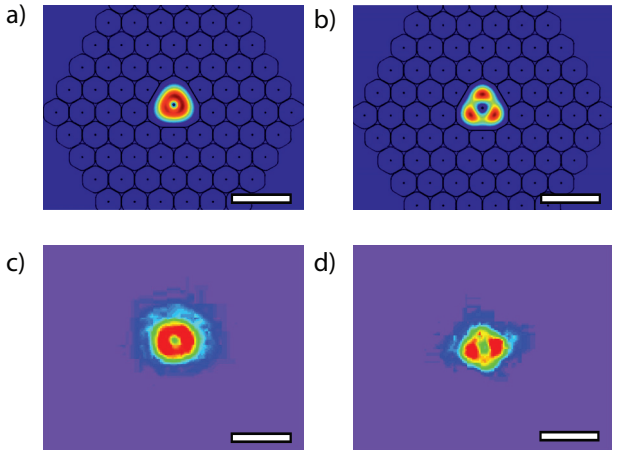

Figure 7. Finite element simulations of the ZnSe MOF shown in Figure 5a, where (a) is the fundamental mode and (b) is the second order mode calculated at 1550 nm. Experimental waveguiding experiments at 1550 nm show that the fundamental mode (c) and second order mode (d) can be isolated. Scale bars: 10 µm.

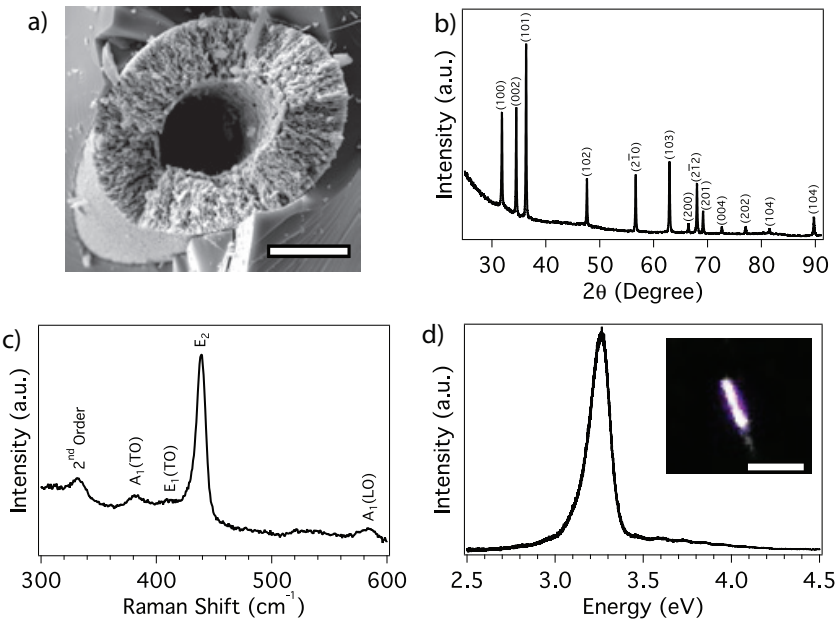

Figure 8. Oxidation of ZnSe to ZnO. a) SEM image of porous ZnO resulting from heating ZnSe in an oxygen ambient. b) XRD reveals that the ZnO is in the hexagonal phase. c) Raman spectroscopy with 488 nm excitation shows the characteristic phonon modes of ZnO. d) Room temperature bandgap photoluminescence (244 nm laser excitation) is observed over the length of a 5 mm long, 50 µm microwire (inset). Scale bars: a) 20 µm and d) inset: 5 mm.

defects and allow for the growth of larger grains. Further reduction in chemical impurities, particularly for ZnS as mentioned previously, could also allow for lower loss.

2.7. Oxidation of ZnSe Templates to ZnO

ZnO has extensive optoelectronic and chemical/catalytic applications due to its wide bandgap and versatile photochemical properties,[14] but HPCVD of oxides has been challenging because many potential chemical routes are inhibited by room temperature pre-reactions. However, an alternative route to ZnO is to use the ZnSe or ZnS microwires as templates that can be oxidized. Annealing of ZnSe in an oxygen ambient (1 atm) at 800–1000 °C results in conversion to ZnO via the following reaction:[51]

$$2ZnSe + 3O_2 \rightarrow 2ZnO + 2SeO_2 \quad (4)$$

At these temperatures, the volatile SeO_2 is readily removed from the capillary via sublimation to result in a ZnO filled capillary (**Figure 8**a). The oxygen annealed material is porous with about 750 nm sized domains, a common morphology resulting from oxidation.[52] XRD reveals that the remaining porous material is crystalline ZnO in the hexagonal phase. There is no indication of residual ZnSe, Se, SeO_2, or metallic Zn (Figure 8b). The ZnO is crystalline, with A_1(TO), E_1(TO), E_2, and A_1(LO) phonon modes present in the Raman spectrum (Figure 8c). The HPCVD ZnSe microwires have low concentrations of impurities and should oxidize to ZnO with similarly low concentrations of impurities. Evidence of the purity of the ZnO microwires is observed in the efficient room temperature bandgap photoluminescence around 3.3 eV (Figure 8d). Further improvement in the materials quality of ZnO could lead to the development of room temperature exciton fiber lasers and piezoelectric tubes that can serve as valves for micro and nanofluidic applications.

3. Conclusions

Our results show how individual pores and designed arrays of pores can be uniformly and conformally coated and filled nearly void-free with II–VI semiconductors by means of HPCVD. The high pressures overcome the mass transport constraints imposed by the very high aspect ratio geometries, such that the transport of precursors into structures with aspect ratios as high as 10^5 can occur. Several HPCVD organometallic reactions have been developed as general routes to II–VI semiconductors. The materials deposit conformally to coat the templates such that the exterior surfaces of the microwires are near atomically smooth and they can guide light with relatively low optical loss (<1 dB/cm) for semiconductor waveguides. The ability to precisely pattern such microwires has allowed for the realization of a microstructured II–VI optical fiber with dual mode guidance. These HPCVD reactions should also be applicable to confined geometries in planar structures, making them useful for applications for which coating of intricate structures is necessary such as photovoltaics, microfluidics, and metamaterials. Layered heterostructures and electrical junctions will also be a natural extension of this work. We anticipate that the reaction chemistries and principles for filling very high aspect ratio structures reported here could be extended to II–VI materials containing Cd, Hg, and Te, the quaternary alloys, and to other families of materials such as III–V semiconductors.

4. Experimental Section

High Pressure Deposition: The partial pressures of $(CH_3)_2Se$, $(CH_3)_2Zn$ (electronic grade, SAFC Hitech), and $(CH_3)_2S$ (99%, Sigma-Aldrich) are about 20 to 40 kPa at room temperature. 70 MPa of hydrogen carrier gas was used to transport the organometallic precursors into the capillary templates. The high pressure precursor mixture is contained in a high strength stainless steel reservoir and configured to flow through a silica capillary template heated to 400–500 °C for 24 h. Proper safety precautions were taken due to the pyrophoric nature of DMZn and flammability of hydrogen. HPCVD is especially safe and practical in small volume reactors for which the total amount of stored precursor and pressure-volume work is minimized.

Materials Characterization: Optical microscopy images were collected with an Olympus BX-62 optical microscope. SEM images and energy dispersive spectra were collected with a FEI Quanta 200 electron microscope. XRD patterns were collected with a Huber G670 imaging plate Guinier camera using Cu$K\alpha_1$ radiation with the entire beam path immersed in helium to reduce background scattering. Raman spectra were obtained in the backscattering geometry with 0.5 mW 488 nm laser excitation using a Dilor XY triple monochromator Raman microscope.

Surface roughness measurements were performed on microwires etched out of the templates with HF (48% w/w) using a Zemetrics ZeScope with a z-direction resolution of 0.01 nm RMS. NaOH (30% w/w) was used to selectively etch grain boundaries of a ZnSe fiber facet at 80 °C. For TEM imaging, the samples were first thinned with gallium ions in a FEI Quanta 200 3D Dual Beam focused ion beam system and then imaged using a Philips (FEI) EM420T transmission electron microscope. The optical transmission losses of the ZnSe fiber waveguides were measured at 1550 nm using the single pass measurement technique. The waveguides, with a typical length of 2–3 cm, were mounted in larger capillaries and polished using standard techniques.

Acknowledgements

The authors acknowledge EPSRC (EP/I035307/1), NSF (DMR-0806860 and DMR-1107894), and the Penn State Materials Research Science and Engineering Center (NSF DMR-0820404) for financial support. They also thank Josh Maier and Dr. Trevor Clark of the Penn State Materials Characterization Lab for assistance with focused ion beam thinning and TEM imaging.

Received: August 7, 2012
Revised: October 10, 2012
Published online: October 30, 2012

[1] R. He, P. J. A. Sazio, A. C. Peacock, N. Healy, J. R. Sparks, M. Krishnamurthi, V. Gopalan, J. V. Badding, *Nat. Photonics* **2012**, *6*, 174.
[2] E. C. Garnett, M. L. Brongersma, Y. Cui, M. D. McGehee, *Annu. Rev. Mater. Res.* **2011**, *41*, 269.
[3] G. M. Whitesides, *Nature* **2006**, *442*, 368.
[4] M. R. Jorgensen, M. H. Bartl, *J. Mater. Chem.* **2011**, *21*, 10583.
[5] C. M. Soukoulis, M. Wegener, *Nat. Photonics* **2011**, *5*, 523.
[6] J. J. Wang, X. Deng, R. Varghese, A. Nikolov, P. Sciortino, F. Liu, L. Chen, X. Liu, *J. Vac. Sci. Technol., B* **2005**, *23*, 3209.
[7] S. M. George, *Chem. Rev.* **2010**, *110*, 111.
[8] R. L. Puurunen, *J. Appl. Phys.* **2005**, *97*, 121301.
[9] L. Reijnen, B. Meester, F. de Lange, J. Schoonman, A. Goossens, *Chem. Mater.* **2005**, *17*, 2724.
[10] J. R. Sparks, R. He, N. Healy, M. Krishnamurthi, A. C. Peacock, P. J. A. Sazio, V. Gopalan, J. V. Badding, *Adv. Mater.* **2011**, *23*, 1647.
[11] D. M. Simanovskii, H. A. Schwettman, H. Lee, A. J. Welch, *Phys. Rev. Lett.* **2003**, *91*, 107601.
[12] S. Mirov, V. Fedorov, I. Moskalev, D. Martyshkin, C. Kim, *Laser Photonics Rev.* **2010**, *4*, 21.
[13] D. U. Bartholomew, J. K. Furdyna, A. K. Ramdas, *Phys. Rev. B* **1986**, *34*, 6943.
[14] U. Ozgur, Y. I. Alivov, C. Liu, A. Teke, M. A. Reshchikov, S. Dogan, V. Avrutin, S.-J. Cho, H. Morkoc, *J. Appl. Phys.* **2005**, *98*, 041301.
[15] P. J. Roberts, F. Couny, H. Sabert, B. J. Mangan, D. P. Williams, L. Farr, M. W. Mason, A. Tomlinson, T. A. Birks, J. C. Knight, P. St. J. Russell, *Opt. Express* **2005**, *13*, 236.
[16] F. Ladouceur, *J. Lightwave Technol.* **1997**, *15*, 1020.
[17] N. Healy, J. R. Sparks, R. R. He, P. J. A. Sazio, J. V. Badding, A. C. Peacock, *Opt. Express* **2011**, *19*, 10979.
[18] T. Y. Fan, *IEEE J. Quantum Electron.* **2005**, *11*, 567.
[19] M. Krishnamurthi, J. R. Sparks, R. He, I. A. Temnykh, N. F. Baril, Z. Liu, P. J. A. Sazio, J. V. Badding, V. Gopalan, *Opt. Express* **2012**, *20*, 4168.
[20] H. B. Callen, *Thermodynamics and an Introduction to Thermostatistics*, John Wiley & Sons, Inc, New York **1985**.
[21] N. F. Baril, R. He, T. D. Day, J. R. Sparks, B. Keshavarzi, M. Krishnamurthi, A. Borhan, V. Gopalan, A. C. Peacock, N. Healy, P. J. A. Sazio, J. V. Badding, *J. Am. Chem. Soc.* **2012**, *134*, 19.
[22] N. F. Baril, B. Keshavarzi, J. R. Sparks, M. Krishnamurthi, I. Temnykh, P. J. A. Sazio, A. C. Peacock, A. Borhan, V. Gopalan, J. V. Badding, *Adv. Mater.* **2010**, *22*, 4605.
[23] A. C. Jones, M. L. Hitchman, *Chemical Vapour Deposition: Precursors, Processes and Applications*, The Royal Society of Chemistry, Cambridge, UK **2009**.
[24] G. B. Stringfellow, *Organometallic Vapor-Phase Epitaxy: Theory and Practice*, Academic Press, San Diego, CA **1999**.
[25] T. Kamins, *Polycrystalline Silicon for Integrated Circuits and Displays*, Kluwer Academic Publishers, Norwell, MA **1998**.
[26] H. Ando, H. Inuzuka, M. Konagai, K. Takahashi, *J. Appl. Phys.* **1985**, *58*, 802.
[27] T. Yokogawa, M. Ogura, T. Kajiwara, *Appl. Phys. Lett.* **1987**, *50*, 1065.
[28] M. Afzaal, M. A. Malik, P. O'Brien, *New J. Chem.* **2007**, *31*, 2029.
[29] W. Kuhn, A. Naumov, H. Stanzl, S. Bauer, K. Wolf, H. P. Wagner, W. Gebhardt, U. W. Pohl, A. Krost, W. Richter, U. Dumichen, K. H. Thiele, *J. Cryst. Growth* **1992**, *123*, 605.
[30] H. Mitsuhashi, I. Mitsuishi, H. Kukimoto, *J. Cryst. Growth* **1986**, *77*, 219.
[31] N. Maung, G. H. Fan, T. L. Ng, J. O. Williams, A. C. Wright, *J. Cryst. Growth* **1996**, *158*, 68.
[32] H. Xu, Y. Liang, Z. Liu, X. Zhang, S. Hark, *Adv. Mater.* **2008**, *20*, 3294.
[33] E. A. Vinogradov, B. N. Mavrin, N. N. Novikova, V. A. Yakovlev, *Phys. Solid State* **2006**, *48*, 1940.
[34] O. Brafman, I. F. Chang, G. Lengyel, S. S. Mitra, E. Carnall, *Phys. Rev. Lett.* **1967**, *19*, 1120.
[35] K. Hayashi, N. Sawaki, I. Akasaki, *Jpn. J. Appl. Phys.* **1991**, *30*, 501.
[36] C. M. Lieber, *Sci. Am.* **2007**, *17*, 64.
[37] J. R. Sparks, J. L. Esbenshade, R. He, N. Healy, T. D. Day, D. W. Keefer, P. J. A. Sazio, A. C. Peacock, J. V. Badding, *J. Lightwave Technol.* **2011**, *29*, 2005.
[38] Y. Jiang, X. Meng, W. Yiu, J. Liu, J. Ding, C. Lee, S. Lee, *J. Phys. Chem. B* **2004**, *108*, 2784.
[39] L. Zhao, Q. Pang, Y. Cai, N. Wang, W. Ge, J. Wang, S. Yang, *J. Phys. D: Appl. Phys.* **2007**, *40*, 3587.
[40] D. Moore, Z. L. Wang, *J. Mater. Chem.* **2006**, *16*, 3898.
[41] H. J. Fan, P. Werner, M. Zacharias, *Small* **2006**, *2*, 700.
[42] N. Healy, L. Lagonigro, J. R. Sparks, S. Boden, P. J. A. Sazio, J. V. Badding, A. C. Peacock, *Opt. Lett.* **2011**, *36*, 2480.
[43] Internal Diameter Measurement of Small Bore Capillary Tubing, http://www.polymicro.com/tech/applicationnotes/appnote_2003JUN.htm (accessed July 2012).
[44] J. Cardenas, C. B. Poitras, J. T. Robinson, K. Preston, L. Chen, M. Lipson, *Opt. Express* **2009**, *17*, 4752.
[45] K. K. Lee, D. R. Lim, L. C. Kimerling, J. Shin, F. Cerrina, *Opt. Lett.* **2001**, *26*, 1888.
[46] K. K. Lee, D. R. Lim, H. Luan, A. Agarwal, J. Foresi, L. C. Kimerling, *Appl. Phys. Lett* **2000**, *77*, 1617.
[47] J. Ballato, T. Hawkins, P. Foy, B. Yazgan-Kokuoz, C. McMillen, L. Burka, S. Morris, R. Stolen, R. Rice, *Opt. Fiber Technol.* **2010**, *16*, 399.
[48] S. Morris, T. Hawkins, P. Foy, J. Hudson, L. Zhu, R. Stolen, R. Rice, J. Ballato, *Opt. Mater. Express* **2012**, *2*, 1511.
[49] N. Healy, J. R. Sparks, M. N. Petrovich, P. J. A. Sazio, J. V. Badding, A. C. Peacock, *Opt. Express* **2009**, *17*, 18076.
[50] N. Vukovic, N. Healy, A. C. Peacock, *J. Opt. Soc. Am. B* **2011**, *28*, 1529.
[51] O. Maksimov, *Mater. Lett.* **2008**, *62*, 3969.
[52] V. V. Ursaki, V. V. Zalamai, A. Burlacu, C. Klingshirn, R. Monaico, I. M. Tiginyanu, *Semicond. Sci. Technol.* **2009**, *24*, 085017.